LBL-23142
Preprint

Lawrence Berkeley Laboratory
UNIVERSITY OF CALIFORNIA

Materials & Chemical Sciences Division

Center for Advanced Materials



Submitted to Corrosion

# INFLUENCE OF AGING AT 200C ON THE CORROSION RESISTANCE OF ALUMINUM-LITHIUM AND ALUMINUM-LITHIUM-COPPER ALLOYS

C. Kumai, J. Kusinski, G. Thomas, and T.M. Devine

March 1987



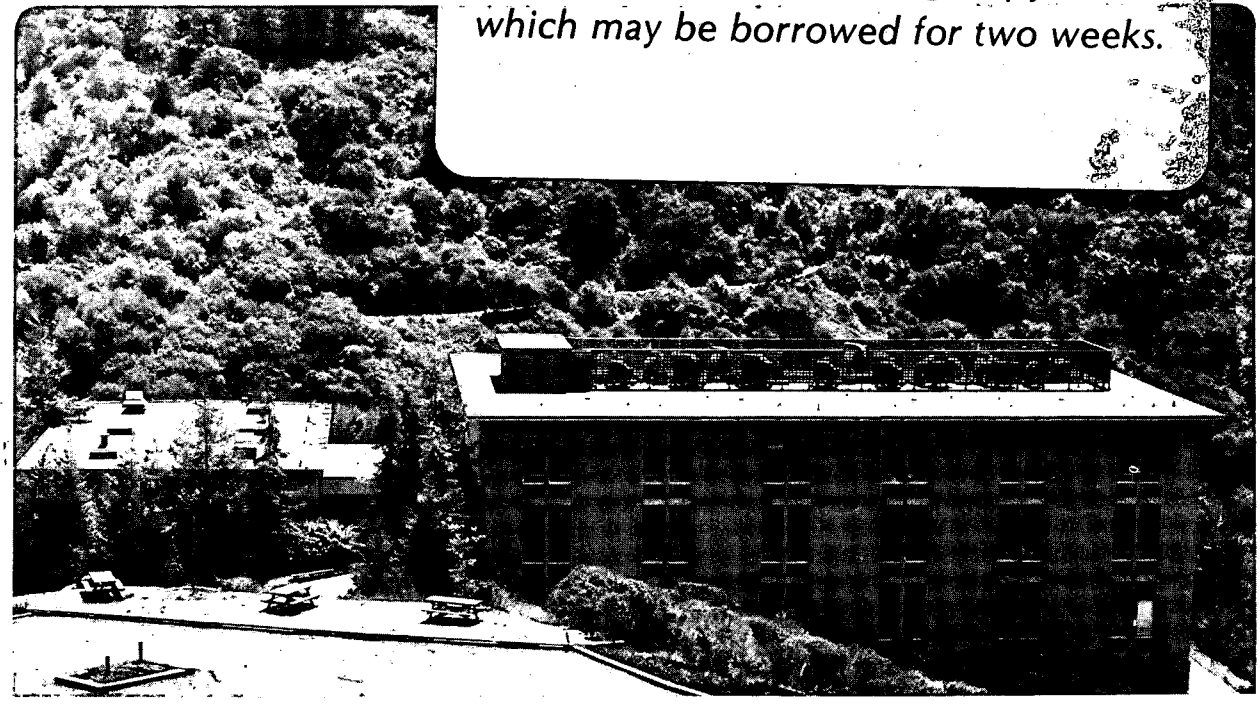

Prepared for the U.S. Department of Energy under Contract DE-AC03-76SF00098

## DISCLAIMER

LBL-23142

# Influence of Aging at 200C on the Corrosion Resistance of Aluminum-Lithium and Aluminum-Lithium-Copper Alloys

C. Kumai, J. Kusinski, G. Thomas, and T.M. Devine

Department of Materials Science and Mineral Engineering
University of California, Berkeley
and
Center for Advanced Materials
Lawrence Berkeley Laboratory
University of California
Berkeley, California 94720

March 1987

# Influence of Aging at 200C on the Corrosion Resistance of Aluminum-Lithium and Aluminum-Lithium-Copper Alloys

C. Kumai[1], J. Kusinski[2], G. Thomas[3] and T. M. Devine[4]
Department of Materials Science and Mineral Engineering
University of California
Berkeley, California 94720
Center for Advanced Materials
Lawrence Berkeley Laboratory

1. Graduate student
2. Post-doctoral Fellow: present address: Institute of Metallurgy
University of Mining and Metallurgy
Al. Mickiewicza #30
Crakow, Poland.
3. Professor
4. Associate Professor

Abstract

The influence of heat treatment on the microstructure and corrosion resistance of an aluminum-lithium alloy and two aluminum-lithium-copper alloys was investigated. Aging the aluminum-lithium alloy resulted in the precipitation of $\delta'$ with PFZ formation along the grain boundaries. The intragranular precipitation of $\delta'$ led to a change in pitting morphology but the magnitude of the pitting potential was unaffected.

Aging the aluminum-lithium-copper alloy resulted in the precipitation of copper-rich phases with PFZ formation along the grain boundaries and subgrain boundaries. EDX microchemical analyses indicated the PFZ was depleted of copper. Anodic polarization of aged samples in chloride-ion media resulted in localized boundary attack. Such attack did not occur in solutions free of chloride ions. The electrochemical tests and microchemical analyses suggest the boundary corrosion was due to the pitting corrosion of copper depleted zones.

## Introduction

The use of aluminum-copper alloys in aqueous media is generally limited to solutions whose pH lies within the range of 4-8.5. In such solutions the passive film formed on the alloys is highly resistant to general corrosion;[1,2] any environmentally-assisted failures usually are the result of localized processes such as pitting corrosion, exfoliation, stress corrosion cracking and corrosion fatigue.

Aircraft structural components are typically exposed intermittently to aqueous environments due to rainfall and condensation effects in humid atmospheres. Because the pH of such aqueous media will usually be within the range in which the passive film is protective the alloy will not suffer from general corrosion. However, because anions such as chloride, sulfate, nitrate, etc. may well be present in the aqueous condensates formed near

sea-coast and industrial locations, localized corrosion processes can occur on structures made of aluminum-copper alloys.

Because of their potential for use in aircraft structural components, the localized corrosion behavior of lithium-containing aluminum-copper alloys must be carefully evaluated. In particular, since such alloys are age-hardenable it is important to understand the effects which precipitation reactions may have on the pitting corrosion and exfoliation resistance of the alloys. One of the important aspects of age-hardening alloys is the inhomogeneity of precipitation resulting from various nucleation phenomena notably heterogeneous precipitation at defects especially grain and subgrain boundaries and the associated adjacent precipitate-free zones (PFZ)[3]. Homogeneous matrix precipitation occurs under high solute atom and vacancy supersaturations. The PFZ's are regions where precipitate nucleation is difficult as a result of vacancy and/or solute atom depletions as they are lost to the nearby sinks.[3-8] The magnitude of this effect is related to the vacancy-solute binding energies, the initial supersaturation and subsequent aging treatments and leads to morphological inhomogeneities which can adversely affect mechanical[3,8,9] and electrochemical properties.[10-12] These effects depend on the diffusion of solutes and hence on the heat treatment. In corrosion, solute-atom depletion is very important because of the highly localized attack that can occur at these regions of inhomogeneity.[10-12] Since lithium is not detected spectroscopically at the resolution limits necessary to identify compositions across PFZs and as no lithium-vacancy binding energy data are available, it is not known whether lithium depletion as well as vacancy depletion occurs at PFZs in Al-Li alloys. On the other hand copper is detectable, e.g. by EDX in TEM/STEM instruments and in Al-Cu alloys the copper-vacancy binding energy is estimated to be ~ 0.2 eV[13] so that the present work seeks to determine the influence of the PFZ morphologies and copper concentration profiles on the pitting and intergranular corrosion resistances of an Al-Li-Cu alloy compared to an Al-Li binary as a function of alloy heat treatment.

## Experimental Procedure

Table I lists the chemical compositions of the alloys investigated along with the compositional specification of alloy 2090. All three alloys were supplied by Alcoa as 1.27 cm thick plate. Alloy A is an experimental Al-Li-Zr composition while alloy B is an experimental Al-Li-Cu-Zr alloy whose composition happens to fall within the specification limits of alloy 2090. The third alloy was supplied by Alcoa and was specified as alloy 2090. Both alloy B and alloy 2090 were received in the T8E41 condition,indicating that each had been solution heat treated, stretched 6% and aged at 163 C for 24 hrs. Note that all three heats contained approximately 0.1 w/0 zirconium for resistance to recrystallization during heat treatment.

Corrosion samples 0.63 cm x 1.27 cm x 2.54 cm were sectioned from

the plate of alloy 2090 with the 1.27 cm length parallel to the rolling direction. Flat tensile samples measuring 10.2 cm long with a 5.1 cm long gauge length and a 0.63 cm x 0.48 cm cross-section in the reduced gauge section were machined from alloys A and B. The tensile specimens were used in a separate study to generate mechanical property data. As described below, corrosion samples for the present study were obtained from the unstrained heads of the tensile samples. The corrosion and tensile samples were ultrasonically cleaned in acetone, wrapped with an inner layer of aluminum foil, an outer layer of tantalum foil, and inserted into a quartz tube. The tube was then alternately evacuated and back-filled with argon several times and then sealed with a 1/4 atmosphere of argon. The inert atmosphere and metal foils were used to limit the loss of lithium during heat treatment and to prevent any interaction between aluminum and the quartz tubes. The encapsulated samples were then solution heat treated at 545C/30 min and water quenched. For aging treatments the samples were again cleaned in acetone, wrapped in an inner layer of aluminum foil and an outer layer of tantalum foil and encapsulated as described above. The samples were water quenched from the aging treatment and dried for subsequent testing.

A 0.63 cm deep hole was drilled through the middle of one of the 0.63 cm x 1.27 cm faces of each corrosion sample of alloy 2090. The hole was then tapped to accept a #5-40 thread. This was used for making electrical contact to the sample during electrochemical testing. The 1.27 cm x 2.54 cm face of each corrosion sample which was perpendicular to both the rolling plane and the rolling direction was metallographically polished to 1/4 micron (μ) diamond finish. A brass rod was then threaded into the sample and the 5 unpolished faces of the specimen were coated with Glyptal paint leaving only the polished surface exposed for testing in a manner which prevented crevice corrosion of the sample. An identical preparation procedure was employed for corrosion samples which were obtained from the heads of fractured tensile samples of alloys A and B. After the Glyptal paint had dried the sample and rod were fitted into a specimen holder, and placed into a glass polarization cell. The sample was located near the geometric center of the cell. There were two 2.54 cm x 5.08 cm platinum-mesh counter electrodes located in the cell and positioned symmetrically about the sample. A saturated calomel reference electrode (SCE) was connected to the cell via a Luggin-Haber probe filled with test solution. The tip of the probe was located within a few millimeters of the sample's surface. Solutions were prepared using analytical reagent grade chemicals and triple distilled water.

Prior to testing, solutions were deoxygenated by bubbling high-purity nitrogen gas through the solution at a rate of 49 liters/hr. for a minimum of 3 hrs. Samples were immersed for 30 min. in the deoxygenated solution and then were anodically polarized at a rate of 1 mV/sec starting at a potential 100 mV less than the corrosion potential. The potential of the sample was controlled by an EG&G PAR potentiostat model 273 equipped

with a model 376 log current converter and a model 175 universal programmer. The data was recorded with an HP 7004B X-Y plotter.

Following corrosion testing the samples were examined for evidence of pitting and general corrosion by viewing each with an optical microscope and a scanning electron microscope.

Transmission electron microscopy studies were carried out in the usual way using foils (from bulk heat treated samples) prepared by electropolishing. Specimens were examined in a Philips EM 301 microscope and in a JEOL 200CX analytical instrument equipped with a thin window EDX detector.

Results

Figure 1(a-c) illustrates the influence of heat treatment and chloride-ion content on the pitting potential of alloy 2090. The two measurements of the pitting potential obtained for each metallurgical condition are plotted and a line is drawn through their average value. Along the horizontal axis the symbols AR and SHT denote, respectively, the as received condition (T8E41) and the solution heat treated condition. The numbers indicate the length of time of aging at 200C following the solution heat treatment. Within the limits of the scatter of the measurements there was no influence of heat treatment on the pitting potential. However, there was a considerable effect of chloride ion concentration with the pitting potential decreasing by ~ 80mV for every factor of ten increase in chloride ion concentration. The data points marked by triangles in the 0.05M NaCl solution were obtained from samples of alloy B. The results for alloy B are seen to be approximately the same as those for 2090 as is to be expected given their similar compositions.

While the pitting potential was relatively insensitive to aging treatment at 200C, the morphology of corrosion attack was strongly influenced by aging. Figure 2 depicts a typical pit formed in 2090 in the T8E41 condition. It consists of a ruptured blister. Pits similar in appearance were found in the solution heat-treated + aged specimens. However, as shown in figure 3a, in the solution heat-treated + aged samples, numerous, isolated regions of boundary attack were also observed. The attack along the boundaries was so discrete that grain dropping occurred leading to the formation of large holes as illustrated in figure 3b.

Figure 4 shows the pitting potentials in 0.05M NaCl obtained from samples of alloy B which were aged for various times at 200 C. Also plotted in figure 4 are the pitting potentials obtained from solution heat-treated + aged samples of alloy A. As the aging time increases to 8 hrs., the pitting potential of alloy B appears to decrease by 50 mV (a small amount) and to remain constant with further aging out to 32 hrs. There appears to be little, if any, influence of aging time at 200 C on the pitting potential of alloy A. Figure 5 illustrates the morphology of a typical pit in alloy A. Strong crystallographic features are apparent. In addition, the attack appears to spread laterally at a greater rate than into the material resulting in wide,

shallow pits.

Figure 6 compares the anodic polarization curves obtained in 0.025M $Na_2SO_4$ and 0.05M NaCl for 2090 heat treated at 200 C for 16 hrs. Optical microscopy of the sample tested in the former solution indicated the absence of localized corrosion and the polarization curve ilustrates that the corrosion rate remains fairly constant as the potential of the sample is increased. The intergranular corrosion and pitting corrosion which occurred in the chloride solution was accompanied by a sharp increase in the corrosion rate above a potential of -550 mV.

Figure 7 depicts the optical microstructures of alloy 2090 in the plane perpendicular to both the rolling plane and the rolling direction. The grains are pancake-shaped which is typical of an aluminum alloy that has been heavily reduced by cold rolling. Figure 8 depicts a transmission electron micrograph of a thin foil of 2090 in the solution heat-treated + 200C/8 hr. condition. There is heavy precipitation of a plate-shaped phase along the subgrain boundaries as well as within the subgrains. A zone which is nearly 0.3μ wide and which is free of these plates lies adjacent to the subgrain boundaries. In addition, spherical shaped precipitates form everywhere in the microstructure including the zone along the subgrain boundaries which is free of the plate phase. Large precipitates were found widely spaced along the grain boundaries. Some of these were complex intermetallic phases containing many impurities.

Figure 9 is a transmission electron micrograph of alloy A, the Al-Li binary, solution heat treated + aged at 200C for 1hr. Large precipitates are present along the grain boundaries. A spherical-shaped precipitate forms homogeneously throughout the microstructure except for a 0.35μ wide precipitate free zone (PFZ) along the grain boundaries. There is no preferential precipitation along the subgrain boundaries nor is there a PFZ along the subgrain boundaries.

Figures 10(a,b) and 11(a,b) depict the STEM/EDX analyses of aluminum and copper contents in alloy B solution heat treated + aged at 200C/32 hrs. as a function of distance along a line which begins within the matrix, crosses the PFZ that runs parallel to the subgrain boundary, crosses the subgrain boundary, the PFZ on the other side and into the matrix. The results indicate that a copper-rich precipitate is forming along the subgrain boundaries and that a zone depleted in copper forms parallel to the subgrain boundaries. The width of the copper depleted zone is measured from the profile of copper concentration with distance to be less than 0.2μ. The width of the PFZ is ~0.1μ. Finally, figure 12 depicts the variation in aluminum and copper concentration with distance along a line which crosses a grain boundary precipitate. The width of the copper depleted zone adjacent to the copper-enriched grain boundary precipitate is ~ 0.2μ.

## Discussion

### Physical Metallurgy

The optical micrographs indicate that the alloys investigated possess the pancake-shaped grain morphology that is typical of rolled aluminum alloys. Apparently the presence of small amounts of zirconium inhibit recrystallization as has been reported by others[14-16] and preserves the as-rolled grain shape even after heat treatments of 545C/30 minutes, WQ. The latter treatment does however produce significant recovery effects and a well developed subgrain structure is formed as is obvious in figure 8.

The transmission electron micrograph in figure 8 of alloy B heat treated at 545C/30 min. + 200C/8 hrs. illustrates the high density of plate precipitates covering the subgrain boundaries and the interior of the subgrains. 0.3μ-wide zones formed on either side of the subgrains are free of these precipitates. This microstructure is very similar to those observed by many workers in aluminum-copper alloys and can be associated with copper vacancy loss to sinks such as subgrain boundaries after quenching and aging.[8,17] One then expects the copper concentration to reach a minimum value as the subgrain boundary precipitates grow and absorb available copper atoms from the vicinity. This is in fact observed in the EDX microanalytical results in figures 10 and 11 which indicate the subgrain boundary precipitate to contain 10-15 w/o copper and reveal the presence of a copper-depleted zone along the subgrain boundaries. A rigorous determination of the identity of the subgrain boundary precipitates was not required in the present study. Rather, their copper contents and that for the surrounding region were sufficient to analyze the cause of corrosion in this alloy as is discussed below. Nevertheless, the works of Silcock[18], Noble et al.[19], Sankaran et al.[15], Tosten et al.[20], and Rioja et al.[21,22] suggest these copper-containing precipitates to be θ' and $T_1$. The former is the tetragonal $Al_2Cu$ phase while the latter is the $Al_2CuLi$ hexagonal phase.

Similarly, the literature[18-22] would designate the metastable phase $Al_3Li$ ( δ') to be the spherical precipitates which form randomly throughout the subgrains including within the zone along the subgrain boundaries which was free of the plate-like precipitate. The formation of δ' within the θ' and/or $T_1$ PFZ along the subgrain boundaries is in agreement with the observation by Gregson and Flower[23] of the absence of a δ'-denuded zone adjacent to $T_1$ precipitates in Al-3Li-1.5Cu and suggests that a lithium-depleted zone does not exist within this θ' and $T_1$ PFZ. Nothing further could be ascertained from the present research concerning whether lithium is depleted in the PFZ. Until methods can be improved to resolve lithium spectroscopically in such regions one simply does not know.

In contrast to the high areal fraction of precipitates along the subgrain boundaries, the grain boundaries of alloy B contained large, well-spaced, copper-containing precipitates as shown in figure 11. While the subgrain

boundaries were outlined by a zone that was free of the plate-like phase but which contained δ', the grain boundaries were rimmed by a true PFZ, void of all secondary phases. As shown by the EDX microchemical analysis in figure 12 the grain boundary PFZ was depleted in copper. This presumably resulted from the formation on the grain boundary of copper-containing phases. Again, it was not possible to determine whether or not lithium-depletion also existed in the grain boundary PFZ.

The secondary phase analyses performed by Noble et al.[24], Williams et al.[25,26], Sanders et al.[27], and Jensrud et al.[28] on Al-Li alloys suggest that the spherical precipitates which formed at random throughout the subgrain structure in alloy A aged at 200 C were δ'. There was no preferential precipitation of δ' along the subgrain boundaries nor was there a PFZ along the subgrain boundaries. There was, however, a PFZ along the high angle grain boundaries. Such a zone must necessarily be depleted of lithium and/or vacancies.

In summary, the microstructures of alloys A and B following aging at 200C are schematically depicted in figure 13. Alloy A contains an almost uniform dispersion of δ' everywhere throughout the microstructure except for a PFZ along the high angle grain boundaries. Similarly, alloy B exhibits a copper-depleted zone and a PFZ along the high angle grain boundaries. In addition, copper-containing phase(s) (presumably θ' and $T_1$) precipitated preferentially along subgrain boundaries as well as intragranularly resulting in copper-depleted zones and θ' and $T_1$ PFZs along the subgrain boundaries.

Corrosion Tests

Ruptured blisters such as that shown in figure 2 were observed in samples of alloy A, alloy B and alloy 2090 which were anodically polarized in chloride-ion solutions. Pits nucleate at these sites. This pitting morphology has been observed in many previous studies and its mechanism of formation has been described.[29]

As shown in figure 4 aging at 200C did cause a small, 50 mV decrease in the value of the potentiodynamic (sweep rate = 1 mV/sec) pitting potential. More importantly, aging at 200C caused dramatic changes in the morphology of the corrosion attack. While samples in the T8E41 condition exhibited only random pitting of the type shown in figure 2, solution heat treatment plus aging induced susceptibility to localized subgrain boundary corrosion and intergranular corrosion as shown in figure 3. The width of the corroded area was extremely narrow. The large holes which formed resulted from the boundary attack dislodging subgrains. The absence of local boundary corrosion in the aged samples which were anodically polarized in 0.025M $Na_2SO_4$ is most interesting and implies that chloride

ions are necessary for the boundary corrosion to occur.

What factors could be responsible for the grain boundary and subgrain boundary corrosion in chloride-ion media? The presence per se of copper-rich phases along the subgrain boundaries is not responsible for the boundary attack. If it were, then enhanced general corrosion should also occur because of the presence of these phases within the grains. This is not observed. In addition, the boundary attack can not be attributed to the $\delta'$ phase that forms in the $\theta'$ and $T_1$ PFZs along the subgrain boundaries as $\delta'$ phase is not present in the regions alongside the high angle grain boundaries, yet localized attack also occurs there. The only feature common to both the high angle grain boundaries and the subgrain boundaries is the copper-depleted zone in the regions immediately adjacent to both types of boundaries.

Could copper-depletion induce susceptibility to corrosion in chloride-ion media? Other researchers have demonstrated that the pitting potential of aluminum increases with increasing amounts of copper.[30-32] Thus the present findings could be explained as being the result of highly localized pitting corrosion of the copper-depleted zones along the subgrain and grain boundaries. In fact, Galvele and DeMicheli[32] have demonstrated that aging aluminum-4w/o copper at 176°C for 3 hours lowers the potentiostatic pitting potential of the grain boundaries relative to that of the matrix by ~100mV. Corrosion testing at potentials above the pitting potential of the grain boundaries resulted in intergranular corrosion of the aged alloy. By demonstrating the influence of copper content on the pitting potential of solution heat treated aluminum-copper alloys tested in chloride-ion containing solutions, and by demonstrating that intergranular corrosion of aged samples of aluminum-4w/o copper did not occur in solutions in which homogeneous, aluminum- low copper alloys did not pit, Galvele et al.[32] inferred that the intergranular corrosion of aged samples of aluminum-4w/o copper was due to the pitting corrosion of a copper-depleted zone along the grain boundaries. In subsequent investigations Sugimoto et al.[33] and Urushino et al.[34] found that aged samples of aluminum-copper alloys were not only susceptible to intergranular corrosion but also were susceptible to intergranular stress corrosion cracking in chloride-ion media. Both studies confirmed the earlier results of Galvele et al.[32] and, like the latter, hypothesized that the intergranular corrosion and intergranular stress corrosion cracking were caused by pitting corrosion of copper-depleted zones along the grain boundaries.

The microchemical analyses performed in the present study clearly demonstrate the existence of copper depleted zones (of the type hypothesized by Galvele et al.[32], Sugimoto et al.[33], and Urushino et al.[34]) along the subgrain and grain boundaries of the aged samples of the aluminum-lithium-copper alloys. Combined with the results of previous studies which demonstrate the influence of copper on the pitting potential

of aluminum alloys[30,31], it is concluded that the intergranular corrosion susceptibility induced by aging at 200°C is the result of localized pitting corrosion of copper depleted zones along subgrain and grain boundaries. To further verify this model, anodic polarization tests conducted in a solution containing chloride-ions (0.05M NaCl) were compared to tests performed in a solution free of chloride ions. The results are presented in figure 6. The sharp increase in corrosion rate at potentials greater than -600mV in 0.05M NaCl was due to localized subgrain boundary corrosion of the type shown in figures 3a and 3b. However, no such localized corrosion occurred in 0.025M $Na_2SO_4$ and the corrosion rate remained very low following polarization to potentials as high as +600mV. The need for chloride ions to produce subgrain boundary attack strongly supports the argument that the localized corrosion is due to pitting along the copper-depleted boundaries. That copper depleted zones along the grain boundaries of aged aluminum-4w/o copper and alloy 2024 are thought to be responsible for the intergranular stress corrosion cracking susceptibilities of these alloys in chloride-ion containing media would suggest that the aluminum-lithium-copper alloys investigated in the present study would also be susceptible to IGSCC.[33]

It is interesting to note that the samples of 2090 tested in the T8E41 condition (SHT + 6% stretch + aged at 163C/24 hours) were not susceptible to intergranular corrosion. Apparently the stretching has prevented the formation of copper-depleted zones. The work of Rioja et al.[21] confirms this beneficial action. By stretching the 2090 after SHT, $T_1$ nucleates randomly throughout the microstructure during subsequent low temperature aging treatments. This finding is consistent with the theory that the intergranular corrosion susceptibility of aged samples of 2090 is due to copper-depleted subgrain boundaries.

In agreement with an earlier study by Niskanen et al.[35], aging alloy A at 200 C did not have a large effect on its pitting potential. Preferential grain boundary and subgrain boundary corrosion did not occur in samples of alloy A in either the solution heat treated condition or when aged at 200C. However the morphology of the pitting corrosion attack in samples aged at 200C was dramatically different from similarly aged samples of alloy B and 2090. Aging alloy A at 200C results in the precipitation of δ' phase throughout the microstructure. A PFZ does develop along the grain boundaries but not along the subgrain boundaries. While aging seems to enhance the initiation of pits in alloy A, the pitting potential remains substantially unchanged by aging. Pits appear to nucleate at random throughout the microstructure and have marked crystallographic features. The pitting attack spreads laterally across the surface at a much higher rate than it grows into the material. This is a unique form of pitting corrosion which has also been observed in lithium-free aluminum alloys[36]. At any rate, the results suggest that the precipitation of δ' in the Al-Li binary alloy does not dramatically affect the pitting resistance of the alloy.

This supports the hypothesis advanced above that the presence of δ' is not responsible for the subgrain boundary and grain boundary pitting of solution heat treated + aged 2090.

In examining the influence of heat treatment on the corrosion resistances of alloys A and B and 2090 it seems clear that lithium per se does not adversely affect the intergranular corrosion resistance of aluminum. Rather, it is the formation of secondary phases containing copper and lithium and the strong dependence on nucleating conditions including vacancy concentrations and trapping which leads to heterogenous precipitation and copper depleted zones along the subgrain boundaries and grain boundaries that is responsible for the localized corrosion there. This result is consistent with the study of Moran et al.[37] who found that lithium did not adversely affect the pitting of aluminum. Thus it would seem possible to design corrosion-resistant, lithium-containing aluminum alloys if careful attention is paid to the other alloying additives, such as copper, that are present.

## Summary and Conclusions

1. The pitting corrosion of an Al-Li alloy and an Al-Li-Cu alloy was studied as a function of aging at 200C.

2. Solution heat treatment (SHT) + aging Al-Li-Cu at 200C results in localized subgrain boundary and grain boundary corrosion in chloride-ion media.

3. SHT + aging Al-Li-Cu at 200C results in precipitation of copper-rich phases on the subgrain and grain boundaries and in the formation of zones which are free of copper-rich precipitates along the boundaries. In addition, δ' precipitates throughout the microstructure except within an 0.2μ-wide PFZ along the grain boundaries.

4. Copper-depleted zones adjacent to the subgrain and grain boundaries were revealed by STEM/EDX microchemical analyses.

5. The subgrain and grain boundary corrosion is thought to result from pitting corrosion of the copper-depleted zones adjacent to the boundary. This hypothesis is supported by
   (a) the known favorable effect of copper additions on the pitting potential of aluminum;
   (b) the absence of boundary corrosion in a solution free of chloride ions;
   (c) the absence of boundary corrosion in samples stretched prior to aging -- stretching + aging results in homogenous precipitation and the absence of copper-depleted zones;
   (d) the absence of boundary corrosion in SHT + aged samples of an Al-Li alloy which did not contain copper.

6. The results suggest that lithium additions may be made to aluminum alloys without adversely affecting the alloy's resistance to pitting corrosion.

Acknowledgements

The authors wish to thank Dr. V. Radmilovic and Mr. R. Sawtell for helpful discussions. C. Echer and Wendy Smith assisted with the STEM/EDX microchemical analyses. The alloys investigated were supplied by Alcoa. This research was supported by a grant from the Director, Office of Basic Energy Science, Material Sciences Division of the United States Department of Energy under Contract No. DE-AC03-76SF00098.

REFERENCES


1. J. Draley and W. Rather, J. Electrochem. Soc., 104, 329, 1957.

2. H.H. Uhlig and R.W. Revie, Corrosion and Corrosion Control, 3rd Ed. p.345, J. Wiley and Sons, New York, 1985.

3. G. Thomas and J. Nutting, J. Inst. Met., 88, 81, 1959/60.

4. H.S. Rosenbaum and D. Turnbull, Acta Met., 7, 664, 1959.

5. J.D. Embury and R.B. Nicholson, Acta Met., 13, 403, 1965.

6. G.W. Lorimer and R.B. Nicholson, Acta Met., 14, 1009, 1966.

7. D.W. Pashley, M.H. Jacobs and J.T. Vietz, Phil. Mag., 16, 51, 1967.

8. E.A. Starke, J. Metals, 54, Jan. 1970.

9. A.H. Geisler, Trans. AIME, 180, 245, 1949.

10. R.B. Mears, R.H. Brown and E.H. Dix, Stress Corrosion Cracking of Metals, p.329, ASTM and AIME, 1944.

11. M.S. Hunter, G.R. Frank and D.L. Robinson, Second International Conference on Metallic Corrosion, p.102, NACE, Houston, TX, 1963.

12. B.W. Lifka and D.O. Sprowls, in Localized Corrosion - Cause of Metal Failure, ASTM STP 516, p.120, ASTM, 1972.

13. H. Kimura, A. Kimura and R.R. Hasiguti, Acta Met., 10, 607,1962.

14. K. Dinsdale, S.J. Harris and B. Noble, Proc. 1st Int. Al-Li Conf., p.101, Metall. Soc. AIME, 1981.

15. K.K. Sankaran and J.E. O'Neal, Proc 2nd Int. Al-Li Conf., Metall. Soc. AIME, 1983.

16. T.H. Sanders and E.A. Starke, Proc. 2nd Int. Al-Li Conf., Metall. Soc. AIME, 1983.

17. R.B. Nicholoson, G. Thomas and J. Nutting, J. Inst. Met., 87, 429, 1958/59.

18. J.M. Silcock, J. Inst. Met., 88, 357, 1959/60.

19. B. Noble and G.E. Thompson, Met. Sci. J. 6, 167, 1972.

20. M.H. Tosten, A.K. Vasudevan and P.R. Howell, Proc 3rd Int Al-Li Conf., Metall Soc. AIME, 1985.

21. R.J. Rioja, P.E. Bretz, R.R. Sawtell, W.H. Hunt and E.A. Ludwiczak, Alcoa internal report, to be submitted for publication.

22. R.J. Rioja and E.A Ludwiczak, Proc. 3rd Int Al-Li Conf., Metall. Soc. AIME, 1985.

23. P.J. Gregson and H.M. Flower, Acta Met., 33, 527, 1985.

24. B. Noble and G.E. Thompson, Met. Sci. J. 5, 114, 1971.

25. D.B. Williams and J.W. Edington, Met. Sci., 9, 529, 1975.

26. D.B. Williams and J.W. Edington, Acta Met., 24, 323, 1976.

27. T.H. Sanders, E.A. Ludwiczak and R.R. Sawtell, Mats. Sci. and Eng., 43, 247, 1980.

28. O. Jensrud and N. Ryum, Mats. Sci and Eng., 64, 229, 1984.

29. R.T. Foley, Corrosion, 42, 277, 1986.

30. M.N. Ronjin, V.G. Pedanova, A.I. Golubev and V.I. Koshechukin, Dokl. Akad. Nauk SSSR, 180, 1161, 1968.

31. K. Sugimoto, Y.Sawada and S. Morioka, Trans Jap. Inst. Met., 13, 345, 1972.

32. J.R. Galvele and S.M. DeMicheli, Corros. Sci., 10, 795, 1970.

33. K. Sugimoto, K. Hoshino, M. Kageyama and Y. Sawada, Corros. Sci., 15, 709, 1975.

34. K. Urushino and K. Sugimoto, Corros. Sci., 19, 225, 1979.

35. P. Niskanen, T.H. Sanders, J.G. Rinker and M. Marek, Corros. Sci., 22, 283, 1982.

36. I.L. Muller and J.R. Galvele, Corros. Sci., 17, 995, 1977.

37. J.P. Moran, E.A. Starke G.E. Stoner and G.L. Cahen, Jr., Corrosion '86, paper no. 203, NACE, Houston, March 17-21, 1986.

TABLE I

CHEMICAL COMPOSITIONS OF ALLOYS INVESTIGATED

(Weight Percent)

| Alloy | Li | Cu | Zr |
|---|---|---|---|
| A | 2.45 | 0.02 | 0.11 |
| B | 2.37 | 2.49 | 0.13 |
| 2090 | 2.86 | 2.05 | 0.12 |
| 2090 Specification | 1.9-2.6 | 2.4-3.0 | 0.08-0.15 |

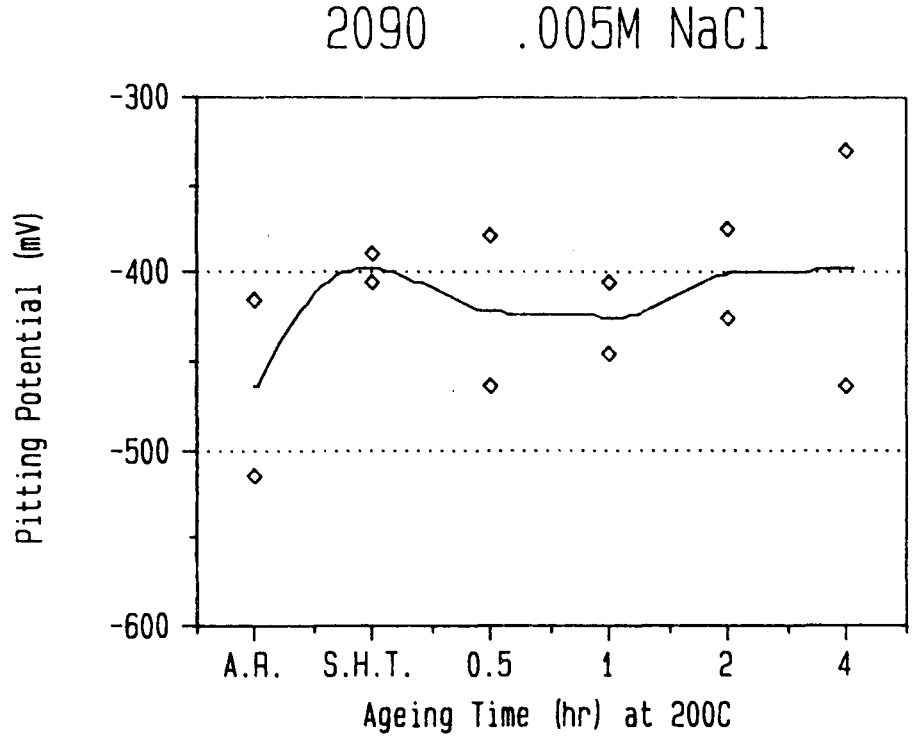


**Figure 1a Influence of heat treatment on the pitting potential of alloy 2090 in 0.005M $Cl^-$**

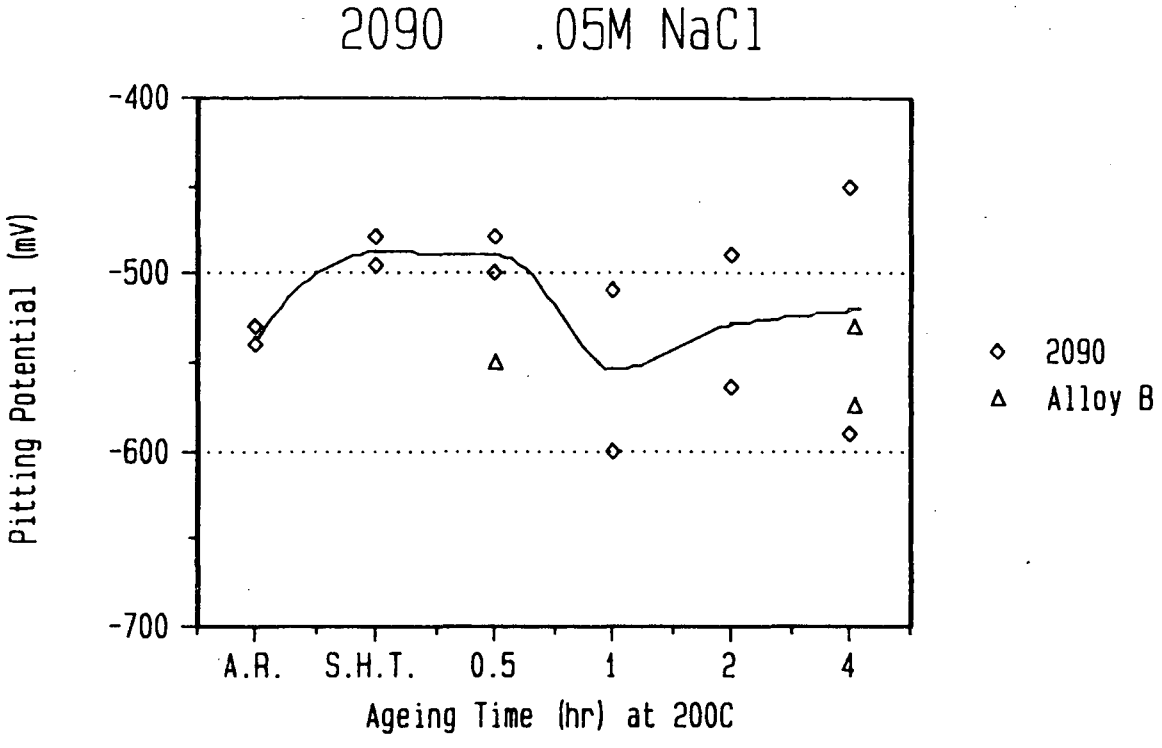


**Figure 1b Influence of heat treatment on the pitting potentials of alloy 2090 and alloy B in 0.05M $Cl^-$**

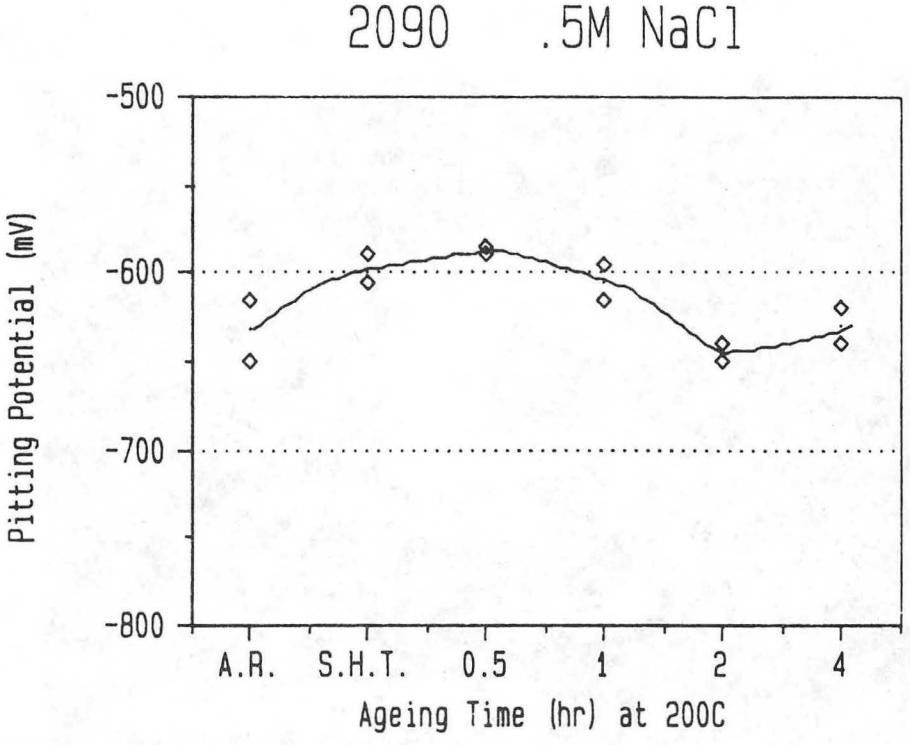


**Figure 1c Influence of heat treatment on the pitting potential of alloy 2090 in 0.5M $Cl^-$**

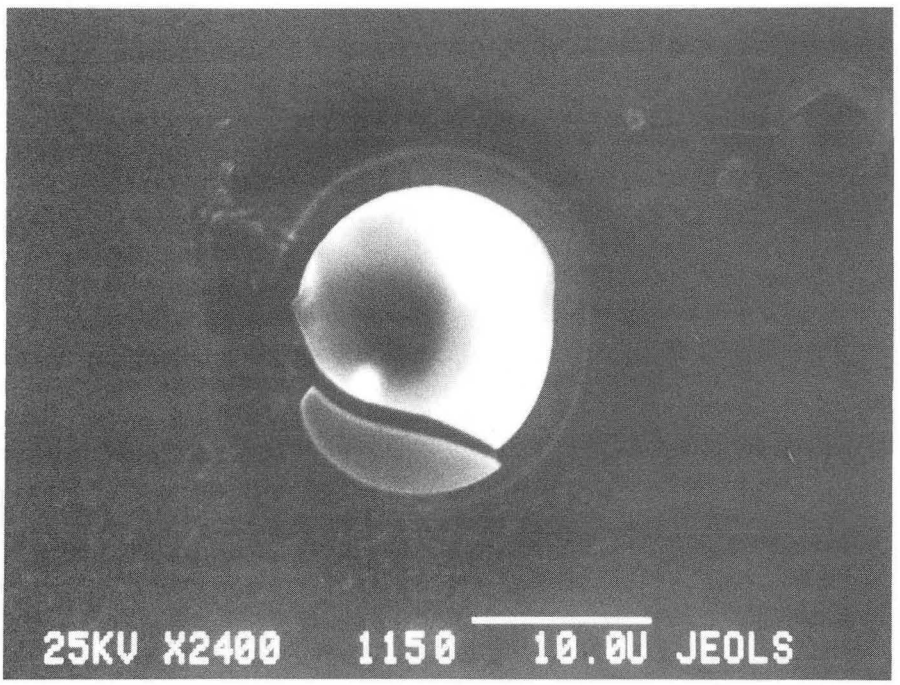


XBB 872-1510

Figure 2 Scanning electron micrograph of ruptured blister in alloy 2090.

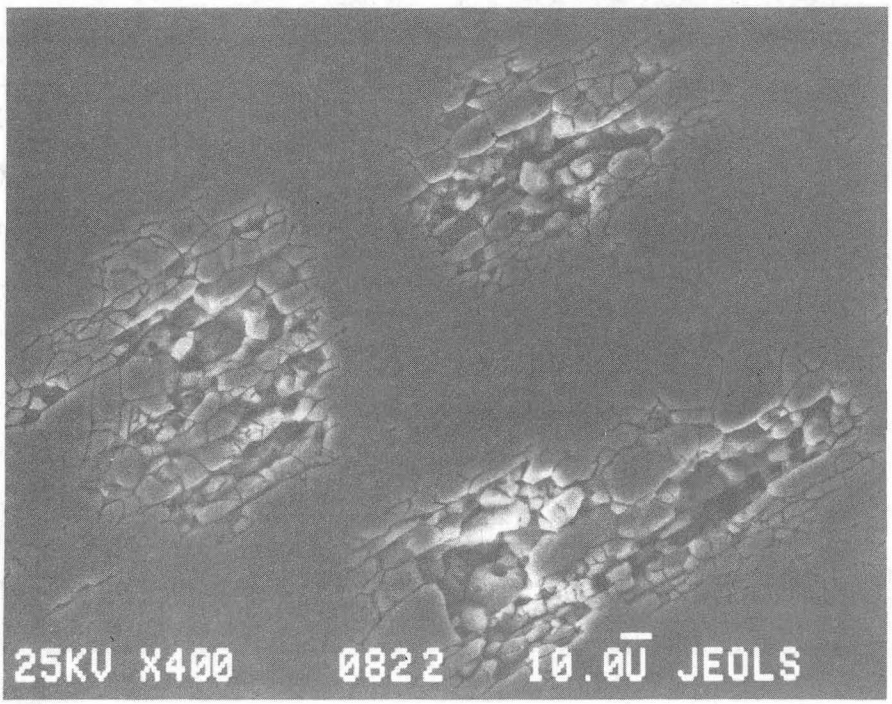


XBB 872-1506

Figure 3a Scanning electron micrograph of subgrain boundary corrosion in alloy 2090 heat treated at 545°/30 min., WQ + 200C/16 hr., WQ.

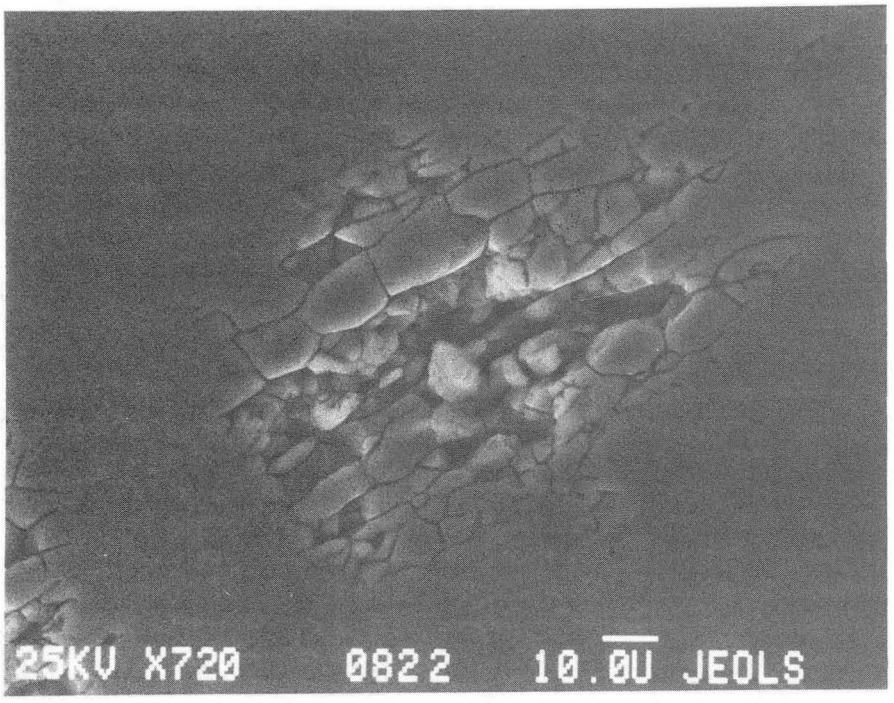


XBB 872-1507

Figure 3b Scanning electron micrograph of subgrain boundary corrosion in alloy 2090 heat treated at 545°30 min., WQ + 200C/16 hr., WQ.

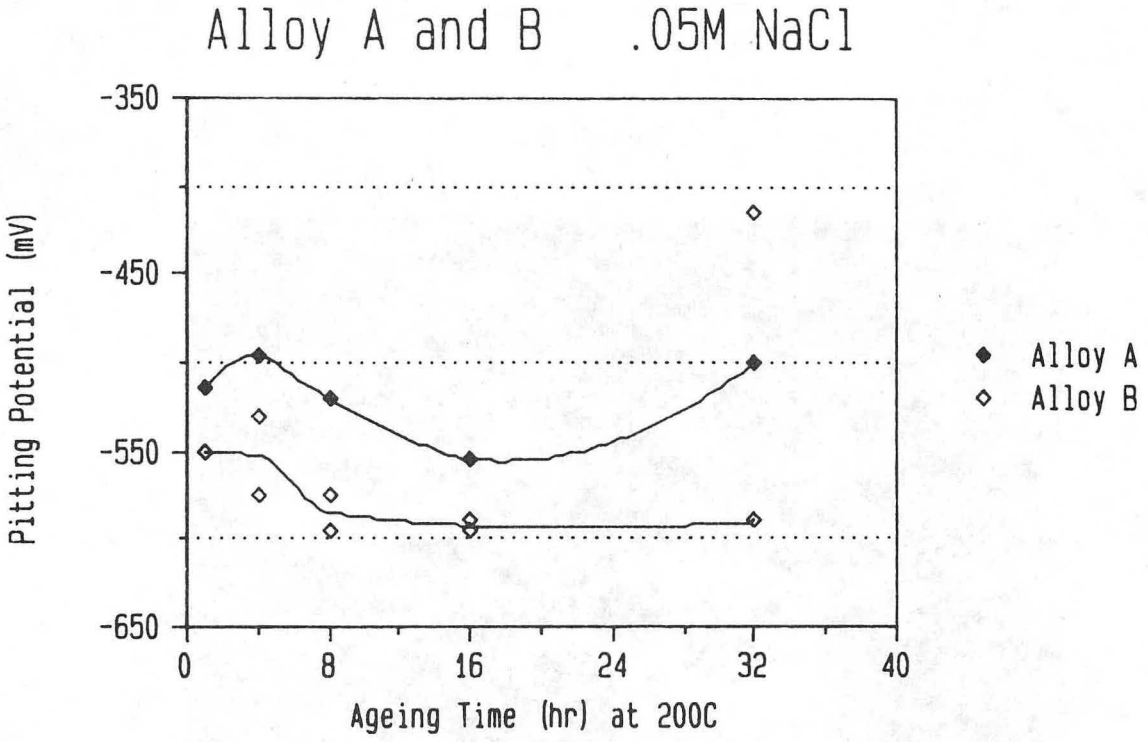


**Figure 4 Influence of heat treatment on the pitting potential of alloys A and B.**

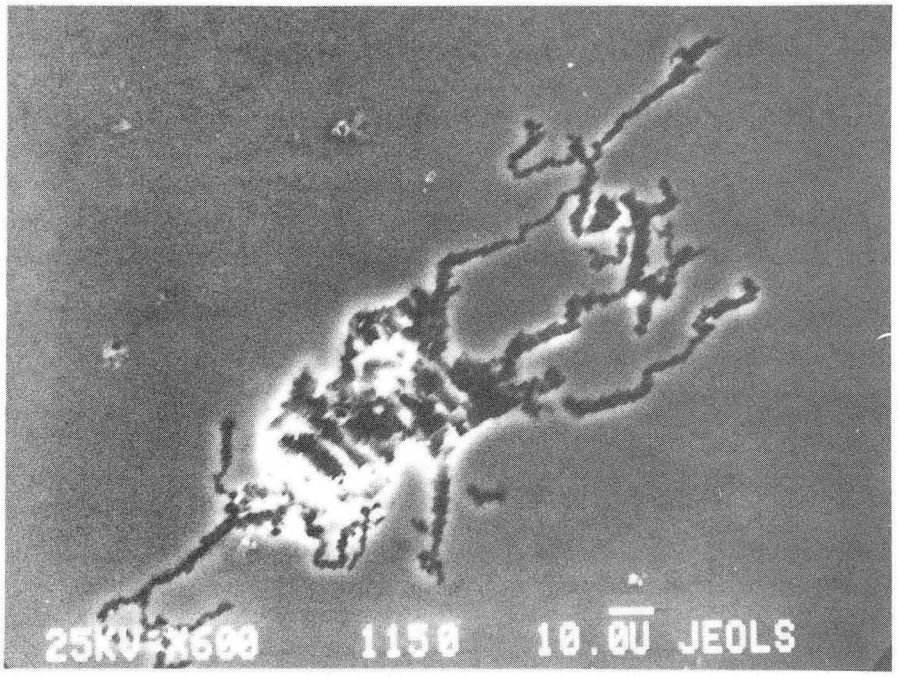


XBB 872-1509

Figure 5 Scanning electron micrograph of pit in sample of alloy A heat treated at 545C/30 min., WQ + 200C/16 hr., WQ.

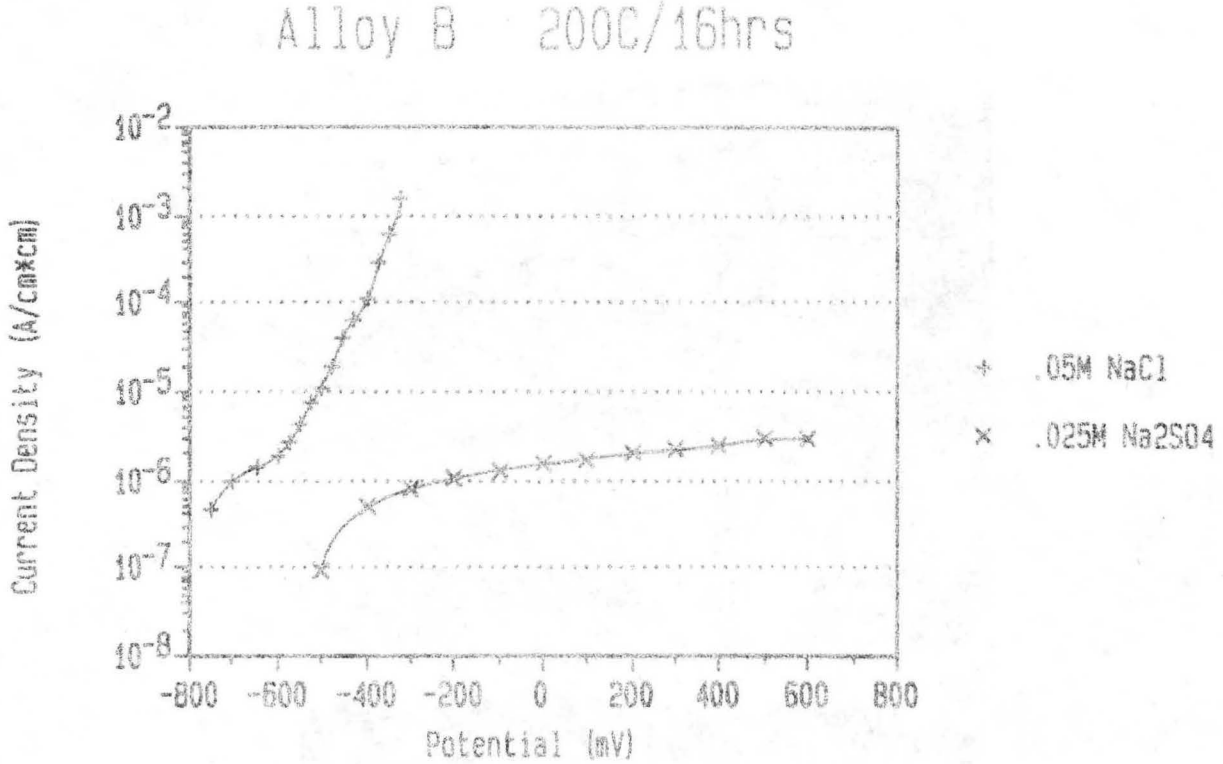


Figure 6 Anodic polarization behavior in 0.05M NaCl and 0.025M $Na_2SO_4$ of alloy B aged at 200 C/16 hrs.

XBB 872-1508

Figure 7 Optical micrograph of through-the-thickness plane of alloy 2090.

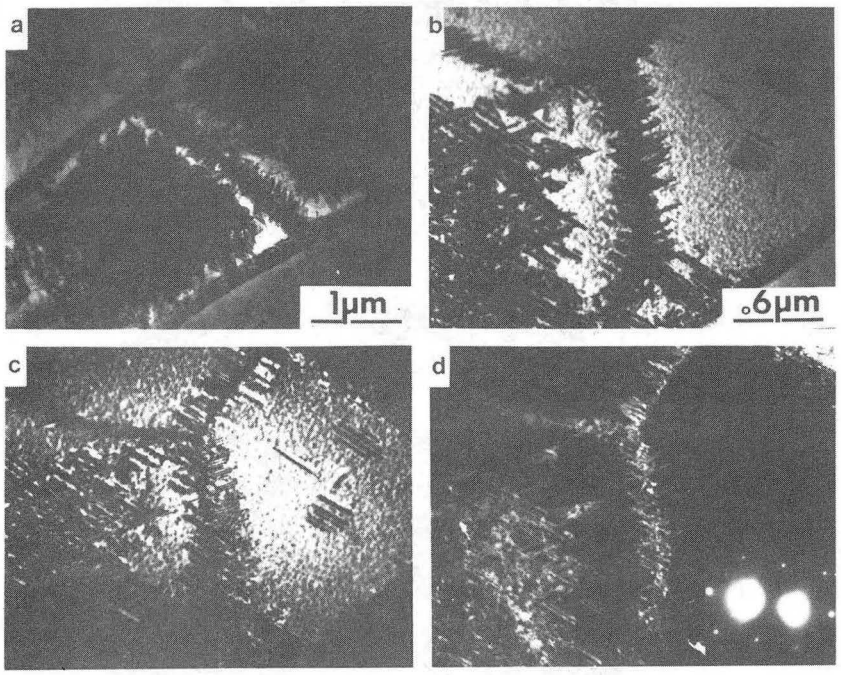


XBB 866-5019

Figure 8 Transmission electron micrograph of alloy B following heat treatment at 550C/30min., WQ, + 200C/8hr., WQ.

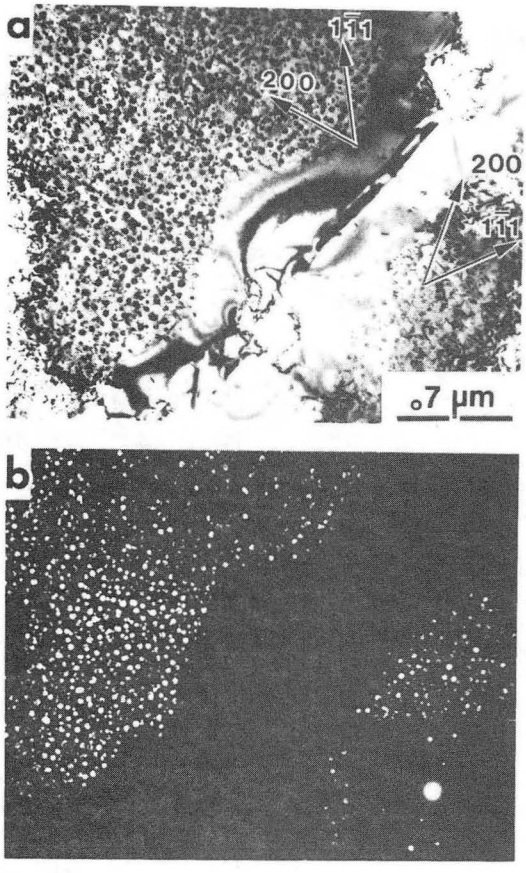


XBB 866-5013

Figure 9 Transmission electron micrograph of alloy B heat treated at 550C/30min., WQ, + 200C/1 hr, WQ, illustrating precipitation along subgrain boundaries and within subgrains.

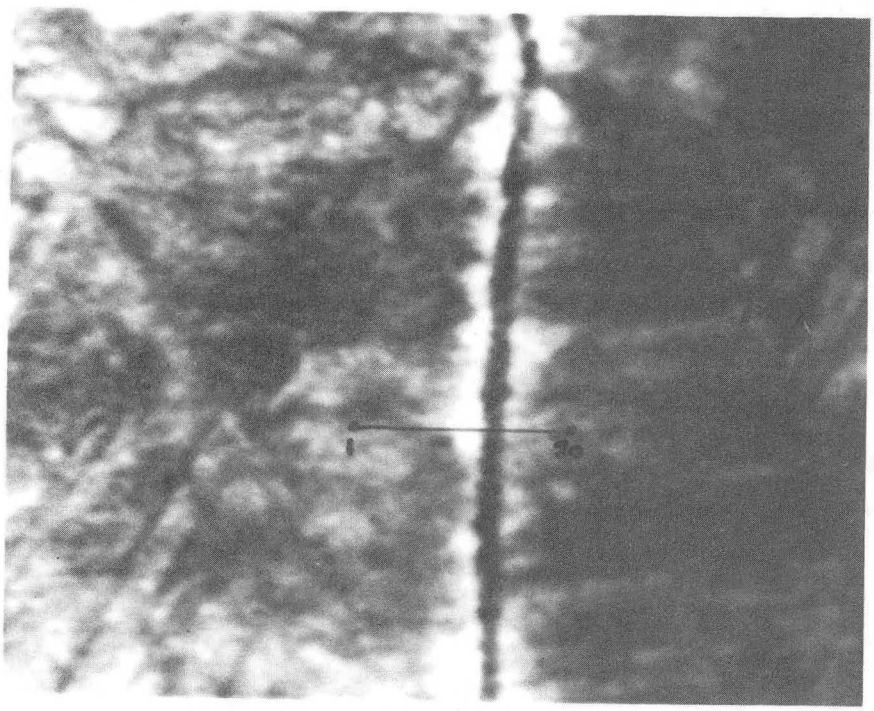

XBB 872-1091

Figure 10a Bright-field transmission electron micrograph of subgrain boundary region (alloy B, 550C/30min., WQ + 200C/32hrs., WQ) microchemically analyzed in figure 10b.

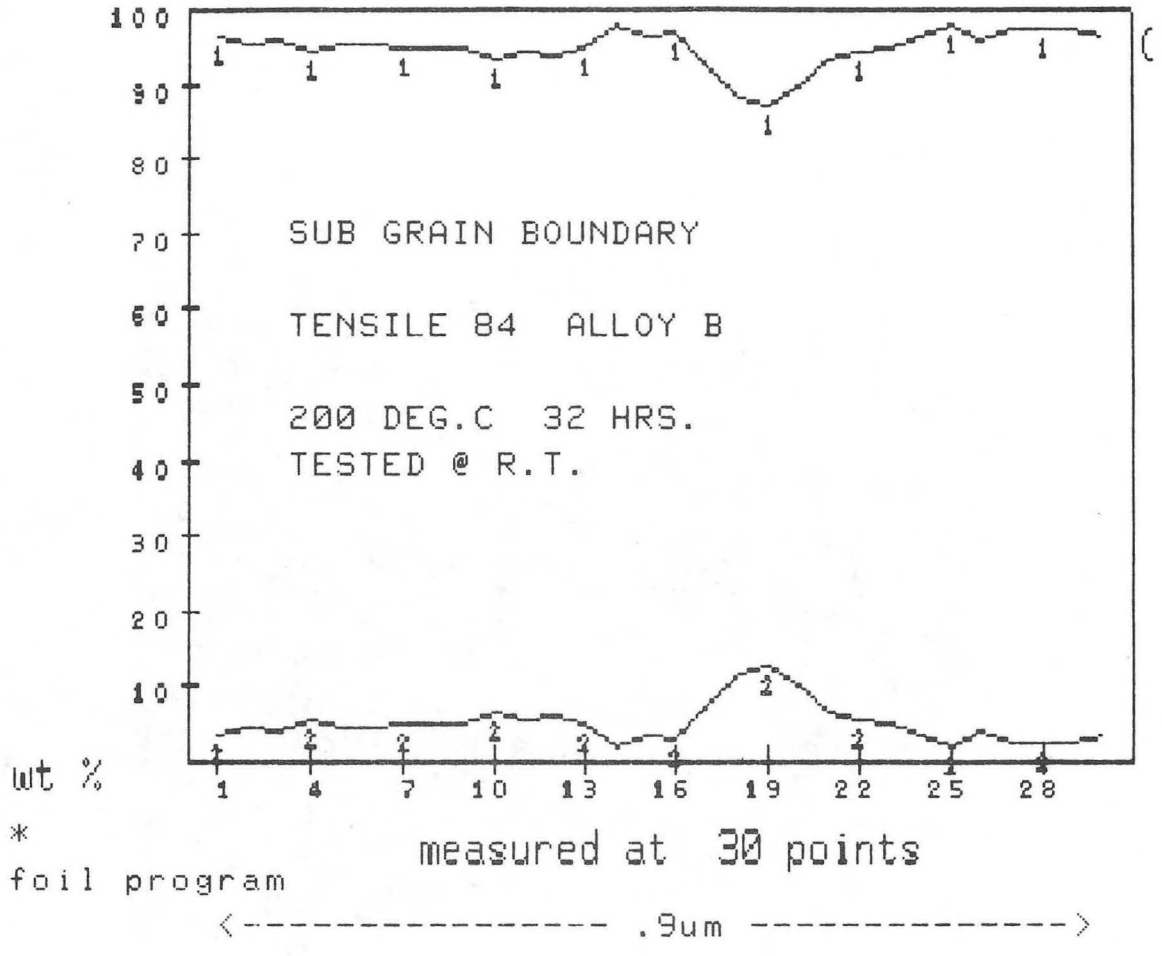


**Figure 10b STEM/EDX analyses of aluminum and copper along a line perpendicular to subgrain boundary in alloy B heat treated at 550C/30min., WQ, + 200C/32 hrs., WQ.**

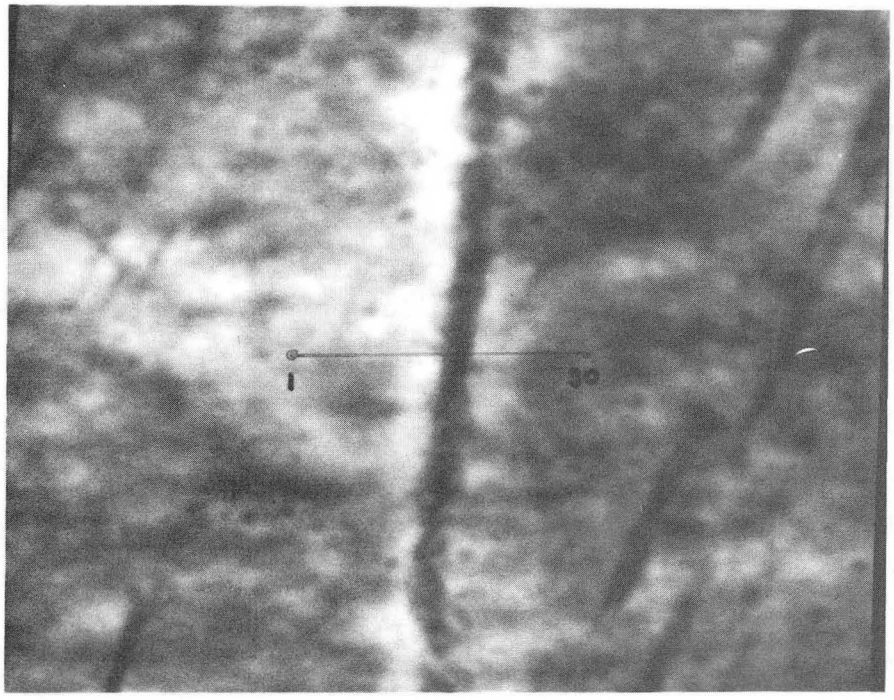


XBB 872-1092

Figure 11a Bright-field transmission electron micrograph of subgrain boundary region (alloy B, 550C/30min., WQ + 200C/32hrs., WQ) microchemically analyzed in figure 11b.

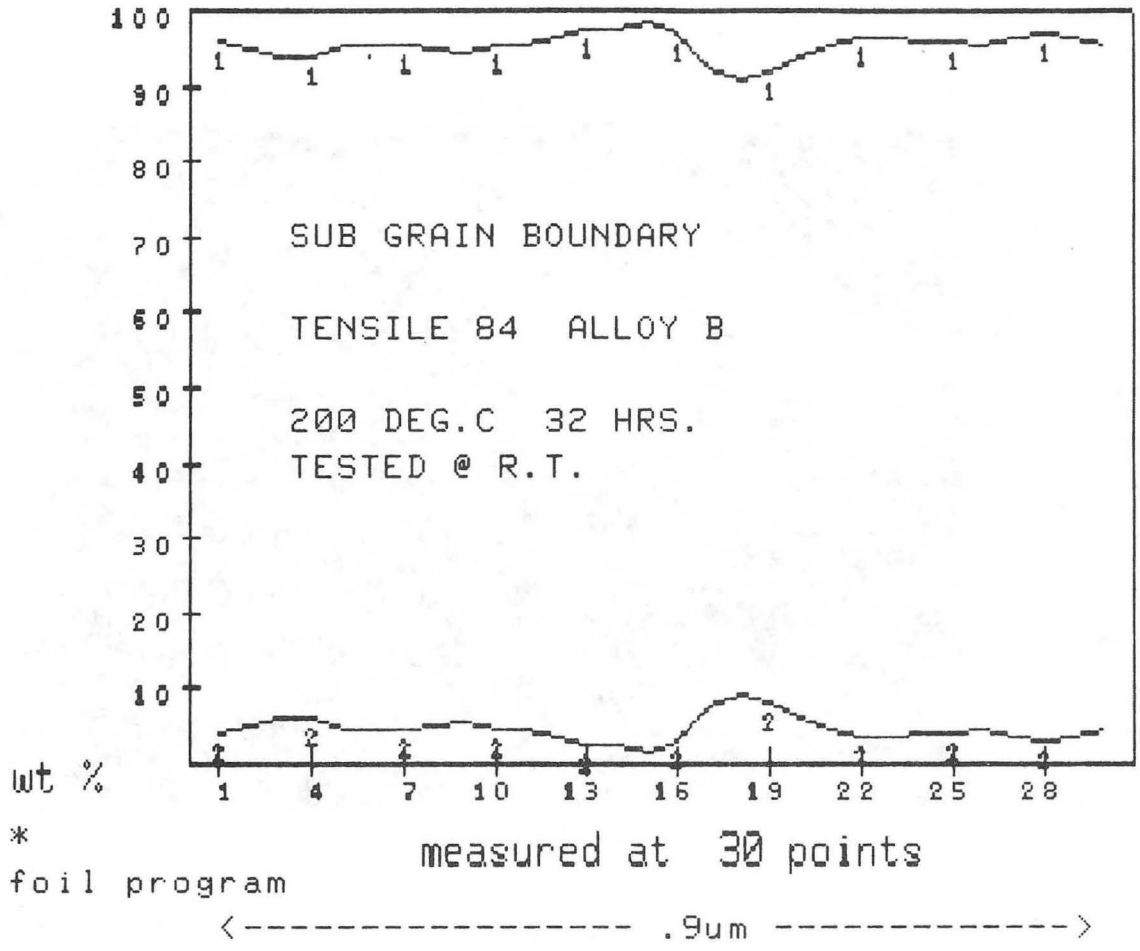


**Figure 11b STEM/EDX analyses of aluminum and copper along a line perpendicular to subgrain boundary in alloy B heat treated at 550C/30min., WQ, + 200C/32 hrs., WQ.**

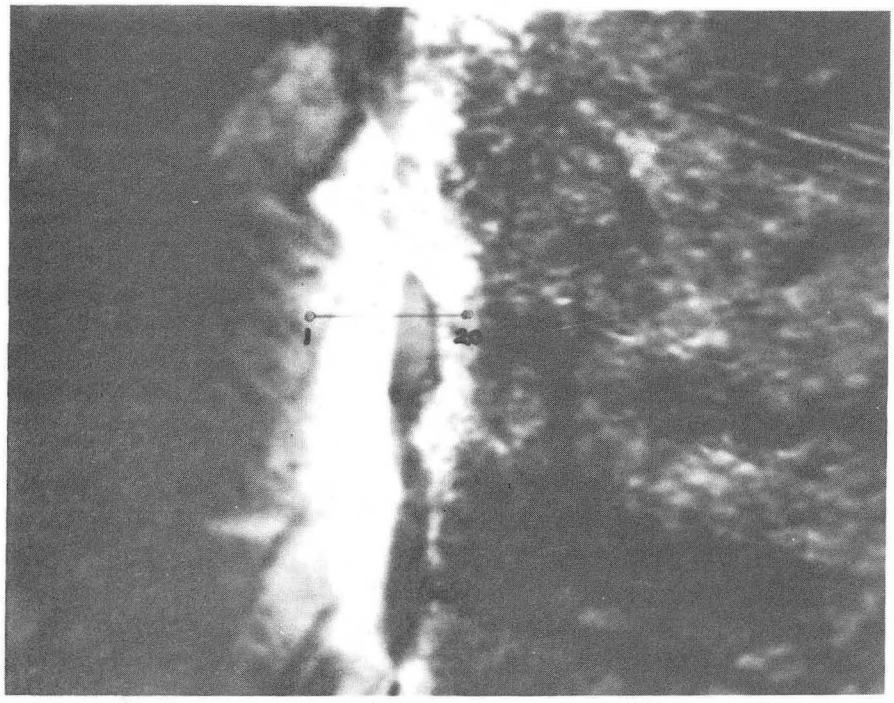

XBB 872-1090

Figure 12a Bright-field transmission electron micrograph of grain boundary region (alloy B, 550C/30min., WQ + 200C/32hrs., WQ) microchemically analyzed in figure 12b.

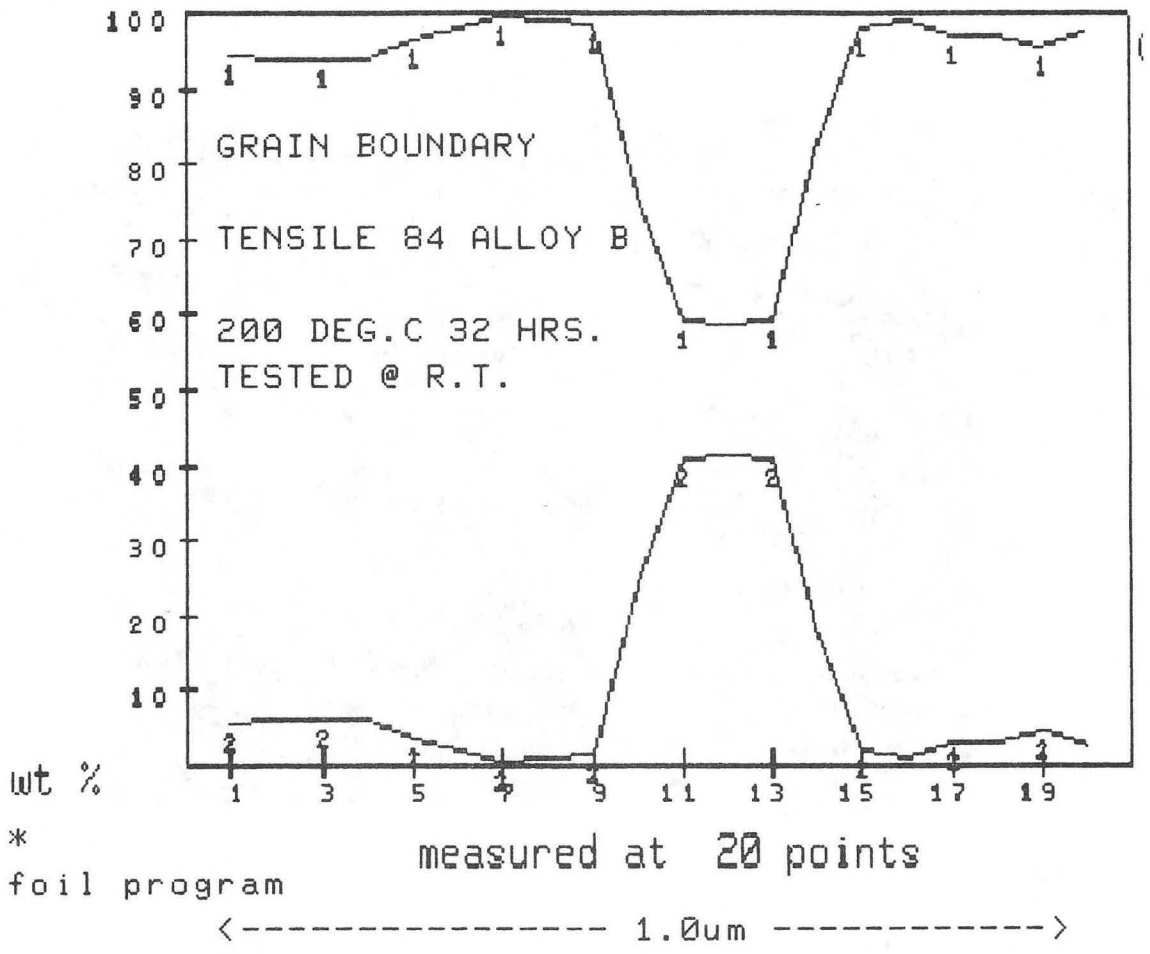


Figure 12b STEM/EDX analyses of aluminum and copper along a line perpendicular to grain boundary in alloy B heat treated at 550C/30min., WQ, + 200C/32 hrs., WQ.

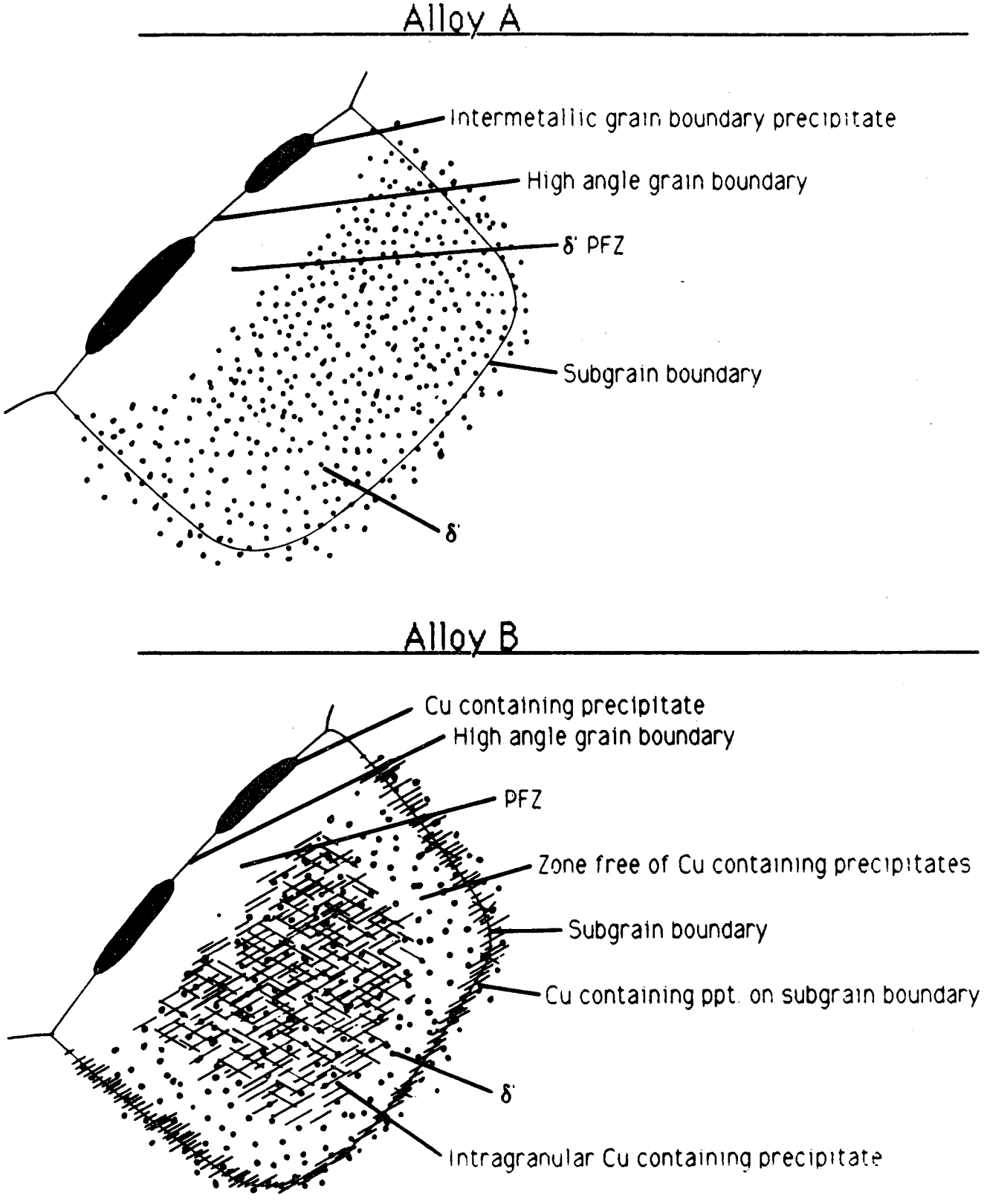


**Figure 13 Schematic illustration of the phase changes occurring within alloys A and B as a result of solution heat treatment + aging at 200C.**

*LAWRENCE BERKELEY LABORATORY*
*TECHNICAL INFORMATION DEPARTMENT*
*UNIVERSITY OF CALIFORNIA*
*BERKELEY, CALIFORNIA 94720*